Tight-binding simulation of optical gain in h-BCN for laser application

Daisuke Maki, Matsuto Ogawa and Satofumi Souma†
Department of Electrical and Electronic Engineering, Kobe University, Kobe 657-8501, Japan
†email: ssouma@harbor.kobe-u.ac.jp

***Abstract*—We present a numerical study on the optical gain in semiconductor laser structure with h-BCN as an active layer. By using the tight-binding method along with the drift-diffusion-Poisson equations, we analyze the optical gain spectra for various band gap energies in h-BCN, demonstrating that the largest gain peak of h-BCN is in the mid-infrared region and can be significantly greater than that in the case of conventional semiconductor active layer.**

I. Introduction

In the research field of semiconductor lasers, there are several important key challenges, such as lower power operation and the wider range of wavelength controllability [1]. Especially semiconductor lasers in mid-infrared region is important in various applications such as defense, industry, communication including IoT, medical care, and healthcare. From the material view point, on the other hand, two-dimensional materials have attracted significant attention owing to their extraordinary electronic properties, promising for various applications in optoelectronics. While graphene is a typical 2D material with a planar honeycomb lattice structure with carbon atoms, its zero bandgap nature is a serious limitation in its optoelectronic applications [2]. For the optoelectronic application of a 2D material, materials with a controllable bandgap is desired. One of the possible strategies is to construct a honeycomb lattice structure consisting of C, B and N atoms [3]. Recently, such material (h-BCN) has been successfully synthesized experimentally [4]. With such background, we explore the possibility of using h-BCN as an active layer material for semiconductor lasers, with the special attention to the gain and wavelength controllability by changing the BN composition x in h-$(BN)_xC_{1-x}$.

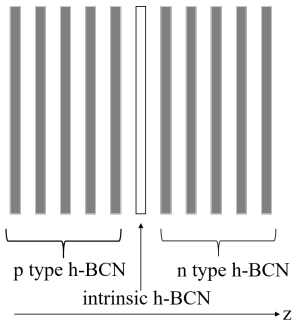

Fig. 1. Schematic illustration of h-BCN multilayer structure assumed in this study.

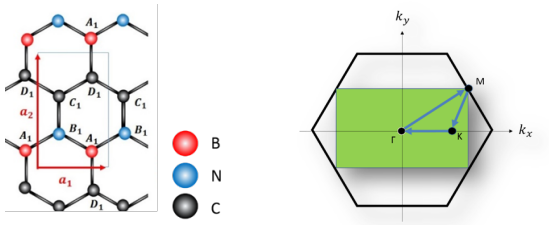

Fig. 2. (Left) Crystal structure of h-BC_2N . (Right) The first Brillouin zone of h-BC_2N (rectangular region). Hexagonal region in the right panel is the first Brillouin zone in the VCA treatment (see Fig. 4).

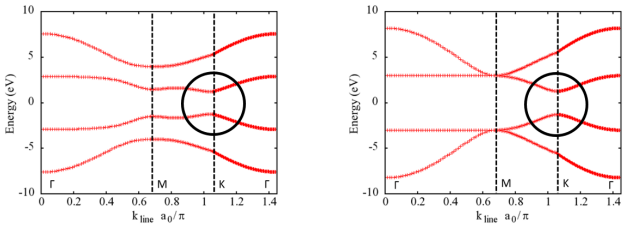

Fig. 3. (Left) Band structure of h-BC_2N calculated using conventional TB method. (Right) Band structure of h-BC_2N calculated based on VCA-TB method.

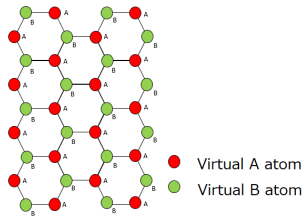

Fig. 4. Crystal structure of h-BCN assumed in VCA.

II. Device structure and calculation method

A. Multilayer h-BCN structure

In this study we assume the h-BCN multilayer structure as shown in Fig. 1, where the central monolayer is intrinsic h-BCN, while the left and the right remaining layers are p- and n-doped h-BCN, respectively. Here assume that different h-BCN layers are quasi independent. That is, although there exist finite overlap of electronic wavefunction between adjacent layers so that the electronic current can flow along the layer direction, the strength of the inter-layer coupling is enough small such that the electronic band structure can be calculated approximately assuming that each layer is independent from others.

Such assumption can be justified in the case of turbostratic multilayer structures [5].

B. Tight-binding approximation method for h-BCN

One of the representative crystal structures of h-BCN is h-BC_2N structure shown schematically in Fig. 2 (left). The corresponding energy band structure can be calculated based on the tight-binding (TB) approximation method, where the wave function of an electron is expanded by linear combination of atomic orbitals, taking into account the overlap of atomic orbitals only between neighboring atoms. In Fig. 3 (left) we plotted the energy band structure of h-BC_2N calculated based on the TB method along the Γ, M, K, and Γ points in the first Brillouin zone (rectangular area) shown in Fig. 2 (right), where we employed TB parameters listed in Ref. [6]. In the study of electronic and optical properties, the band structure near the band edges (bottom of the conduction band and the top of the valence band) is essentially important. In the case of h-BCN, the band edges are positioned at the K point as enclosed by circle in Fig. 3 (left).

C. Validity of virtual crystal approximation

Although the above mentioned conventional TB approach is useful to predict precisely the band structures of various specific crystal structures of h-BCN where CC pairs in graphene are replaced by BN pairs in specific ways [7], [8]. On the other hand, for the purpose of understanding how the characteristics of h-BCN-based electronic/optical devices depend on the BN composition x in graphene, the use of virtual crystal approximation (VCA) is useful [9], where the unit cell is kept as the primitive unit cell of graphene (containing two atoms) and the TB parameters (on-site and hopping energies) are replaced by the averaged values between graphene and h-BN with the BN composition ratio x. That is, the on-site energies of boron-like and nitrogen-like virtual atoms [virtual A and B atoms in Fig. 4] are $\varepsilon'_{\rm B} = x\varepsilon_{\rm B} + (1-x)\varepsilon_{\rm C}$ and $\varepsilon'_{\rm N} = x\varepsilon_{\rm N} + (1-x)\varepsilon_{\rm C}$, respectively, and the hopping energy between these boron-like and nitrogen-like virtual atoms is $t'_{\rm BN} = xt_{\rm BN} + (1-x)t_{\rm CC}$, where the on-site energies of pure boron, nitrogen, and carbon are $\varepsilon_{\rm B} = 2.46$ eV, $\varepsilon_{\rm N} = -2.55$ eV, and $\varepsilon_{\rm B} = 0$ eV, respectively, and the B-N and C-C hopping energies are $t_{\rm BN} = -2.16$ eV and $t_{\rm BN} = -2.7$ eV, respectively. Then the electronic properties of each h-$(BN)_xC_{1-x}$ layer can be calculated by solving the eigenvalue problem $H(\boldsymbol{k})\,|\psi_{l\boldsymbol{k}}\rangle = E_l(\boldsymbol{k})\,|\psi_{l\boldsymbol{k}}\rangle$ [$l = 1$ (2) corresponds to the valence (conduction) band] with the Hamiltonian

$$H(\boldsymbol{k}) = \begin{pmatrix} \varepsilon'_{\rm B} & h^*(\boldsymbol{k}) \\ h(\boldsymbol{k}) & \varepsilon'_{\rm N} \end{pmatrix}, \tag{1}$$

$$h(\boldsymbol{k}) = -t'_{\rm BN}\left(2e^{ik_y a_0/2}\cos(k_x\sqrt{3}a_0/2) + e^{-ik_y a_0}\right). \tag{2}$$

Figure 3 (right) shows the band structure of h-BC_2N (corresponding to the BN composition $x = 0.5$) calculated using VCA-TB method. By comparing the band structures of h-BC_2N calculated using the conventional TB [Fig. 3(left)] and VCA-TB [Fig. 3(right)] near the band edges (enclosed by circles), it can be seen that both have the same band gap at the K point and the similar band dispersion, indicating the validity of VCA.

D. Difference of quasi Fermi levels for holes and electrons

Next step is to obtain the difference of the quasi Fermi levels between the holes and electrons at the central active layer, calculated by solving the drift-diffusion (DD) equation along with the Poisson's equation:

$$\frac{dc_j(z,t)}{dt} = -\frac{d}{dz}F_j(z,t) + r_j(z,t), \tag{3}$$

$$F_j(z,t) = -D_j\frac{dc_j(z,t)}{dz} + c_j(z,t)q_jM_j\left(-\frac{d\varphi(z,t)}{dz}\right), \tag{4}$$

$$-\frac{d}{dz}\varepsilon(z)\frac{d\varphi(z,t)}{dz} = q_+\left(c_+(z,t) + N_{\rm D}^+(z)\right) + q_-\left(c_-(z,t) + N_{\rm A}^-(z)\right). \tag{5}$$

Here $c_j(z,t)$ is the hole/electron density ($j = +/-$), $F_j(z,t)$ is the flux density along the z-direction (layer direction), $r_j(z,t)$ is the reaction (generation+recombination) rate, $\varphi(z)$ is the electrostatic potential, D_j is the diffusion coefficient, $M_j = D_j/k_BT$ is the mobility, $q_\pm = \pm e$, and $N_{\rm D/A}^{+/-}$ are the ionized donor/acceptor densities. We employed the relaxation time approximation for the reaction term with the relation time $\tau = 1$ ps. Other assumed parameters are: the doped charge density ± 0.01 in units of $e(>0)$ per unit cell per layer for n/p-doped region and the interlayer mobility 10^{-12} m^2/Vs.

In our simulations the hole and electron densities $c_\pm(z,t)$ in the DD equations (3) and (4) are self-consistently calculated not only with the Poisson's equation Eq. (5) but also with the hole and electron densities calculated using the band structure profiles $E_l(\boldsymbol{k}) - e\varphi(z)$ and the local quasi-Fermi levels $E_{\rm Fh/e}(z)$ for holes/electrons, in which $\varphi(z)$ obtained by Poisson's equation and $c_\pm(z,t)$ obtained by DD equations are required, respectively. The above whole self-consistent calculations have been performed based on the Newton's algorithm assuming the steady state.

E. Optical gain in h-BCN active layer

Once the converged quasi Fermi levels $E_{\rm Fh/e}$ for hole/electron are obtained based on the self-consistent procedure mentioned above, the optical gain g in the h-BCN active layer is calculated by the radiation energy $W_{\rm rad}$ per unit area per unit time divided by the incident electromagnetic flux $I_{\rm in}$ as $g = W_{\rm rad}/I_{\rm in}$, where

$$W_{\rm rad} = \frac{2\hbar\omega}{S_{\rm UC}N_k}\sum_{\boldsymbol{k}}\frac{2\pi}{\hbar}\left|H'_{\rm CV}(\boldsymbol{k})\right|^2\delta\left(E_{\rm C}(\boldsymbol{k}) - E_{\rm V}(\boldsymbol{k}) - \hbar\omega\right) \times\left[f(E_{\rm C}(\boldsymbol{k}) - E_{\rm Fh}) - f(E_{\rm V}(\boldsymbol{k}) - E_{\rm Fe})\right] \tag{6}$$

and $I_{\rm in} = n\varepsilon_0 c{E_0}^2/2$. Here $H'_{\rm CV}(\boldsymbol{k}) = \langle\psi_{2\boldsymbol{k}}|H'|\psi_{1\boldsymbol{k}}\rangle$ with H' being the perturbation Hamiltonian due to the coupling between electrons in h-BCN and electromagnetic field (see Ref. [10] for detail).

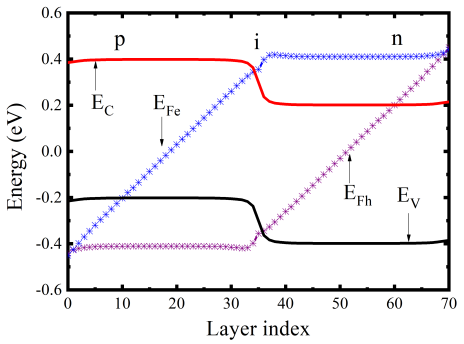

Fig. 5. Band edges ($E_{\rm V}$ and $E_{\rm C}$) and the quasi Fermi levels ($E_{\rm Fh}$ and $E_{\rm Fe}$) as a function of the layer index.

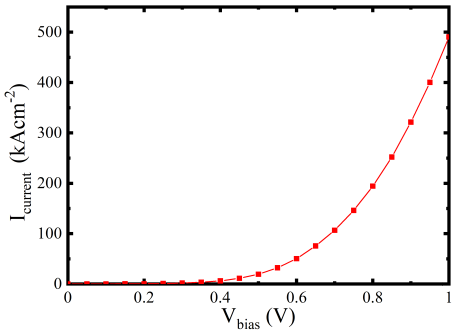

Fig. 6. Forward bias $V_{\rm bias}$ dependence of the current density along the z-direction in Fig. 1 for the BN composition $x = 0.12$.

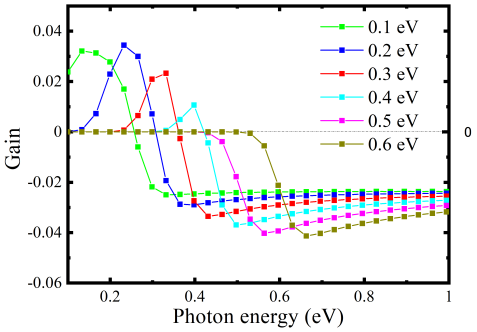

Fig. 7. Photon energy dependence of the optical gain are plotted for various values of the band gap $0.1 \sim 0.6$.

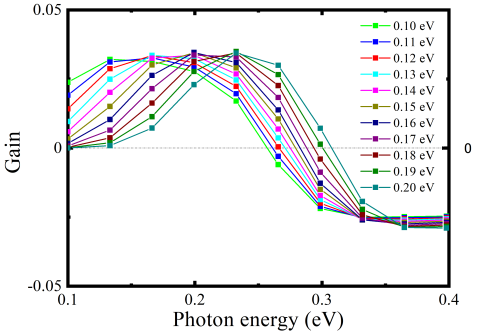

Fig. 8. Photon energy dependence of the optical gain are plotted for various values of the band gap $0.1 \sim 0.2$.

III. Results and Discussions

Figure 5 shows the band edges ($E_{\rm V}$ and $E_{\rm C}$) and the quasi Fermi levels ($E_{\rm Fh}$ and $E_{\rm Fe}$) as a function of the layer index, where the the band gap was set to 0.6 eV (corresponding to the BN composition $x = 0.12$) and the forward bias voltage $V_{\rm bias} = 1$ V was applied over the whole layers. Calculation were made with a total of 71 layers, including 35 p-type cladding layers, 1 active layer, and 35 n-type cladding layers throughout this study. In this figure it can be seen that the quasi-Fermi level difference between holes and electrons is larger than the band gap at the central active layer. We performed the above mentioned calculations for various values of the band gap, and obtained the corresponding quasi-Fermi level differences at the active layer.

In order to clarify the bias voltage range which can be applied in the assumed layer structure, in Fig. 6 we plotted the forward bias $V_{\rm bias}$ dependence of the current density across the pn junction layers. Here we have confirmed that the typical nonlinear I-V behavior can be maintained at least up to the bias $V_{\rm bias} = 1$ V.

Next we analyze the gain spectra in the proposed structures. In Fig. 7, the photon energy dependence of the optical gain are plotted for various values of the band gap $0.1 \sim 0.6$ corresponding to the BN composition $x = 0.02 \sim 0.12$. As can be seen first from the Fig. 7, finite (positive) gain can be realized for the band gap smaller than 0.5 eV, and for the band gap grater than 0.6 eV all incident light is absorbed. This is basically because the quasi Fermi level difference $E_{\rm Fh} - E_{\rm Fe}$ cannot exceed the band gap for such large band gap.

Figure 8 shows the photon energy dependence of the optical gain are plotted for various values of the band gap $0.1 \sim 0.2$ in 0.01 steps corresponding to the BN composition $x = 0.02 \sim 0.04$. The calculated result shows that the maximum gain is obtained at 0.19 eV.

Figure 9 shows the gain spectra for the above mentioned optimized band gap 0.19 eV for various values of total number of layers (including one active layer at the middle), where we have used the self-consistently obtained values of the Fermi level differences (between holes and electrons) listed in Table 1. In Fig. 9 we can see that the gain spectrum is almost independent of the total number of layers. This is consistent with the fact that the change in the quasi Fermi level differences due to the change in the number of layers is negligibly small. Based on the results obtained so far, it is considered that the gain is determined mainly by the difference of quasi Fermi level with respect to the size of the band gap. It is also important to note that the smaller the band gap, the wider the range of photon energy at which the nonzero gain is possible, although the maximum value of gain becomes smaller when the band gap is larger than 0.19 eV. The resultant values of the 2D gain (dimensionless) can be converted to the 3D gain by using the interlayer distance of graphite (3.85 Å), obtaining the largest gain peak of h-BCN (band gap: 0.19 eV) as being 7.14×10^4 cm^{-1}, which is about 178 times larger than that in the commonly used semiconductor AlGaAs as being

4.00×10^2 cm^{-1}.

Table. I
RELATIONSHIP BETWEEN THE NUMBER OF LAYERS AND DIFFERENCE OF QUASI FERMI LEVELS.

The number of layers	Difference of quasi Fermi levels (eV)
31	0.29970
41	0.29904
51	0.29896
61	0.29894
71	0.29894

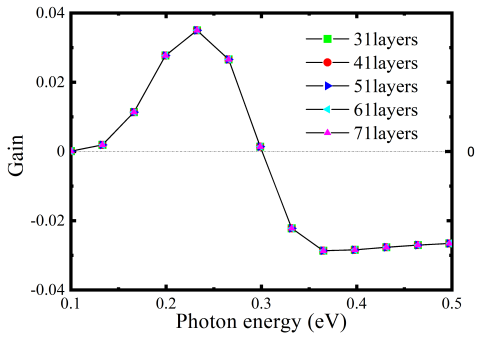

Fig. 9. Photon energy dependence of the optical gain are plotted for various values of layers 31 $\sim$ 71.

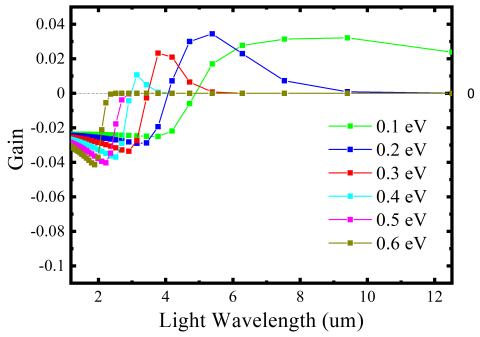

Fig. 10. Wavelength dependence of the optical gain are plotted for various values of the band gap 0.1 $\sim$ 0.6 .

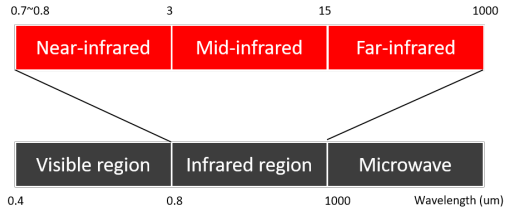

Fig. 11. Wavelength range of light.

Finally in Fig. 10 we plotted the gain spectra for various bandgaps as a function of the light wavelength. From this figure and the schematic diagram in Fig. 11, it is found that the wavelength at which the maximum gain is obtained is in the mid-infrared region, which is important for various applications such as communications including IoT, and health cares.

IV. CONCLUSION

We presented a numerical study on the optical gain in semiconductor laser structure with h-BCN as active an layer. By using the tight-binding formalism, drift-diffusion-Poisson equations, and the Fermi's golden role to calculate the electronic band structure, quasi-Fermi level, and the optical gain, respectively, we analyzed the optical gain spectra for various band gap energies in h-BCN, demonstrating that the largest gain peak of h-BCN can be significantly greater than that in the case of conventional semiconductor active layer. The peak of the gain is in the mid-infrared region, meaning that the proposed material can be applicable for various applications such as communication including IoT and health cares.

ACKNOWLEDGMENT

This work was partially supported by JSPS KAKENHI Grant No. 19H04546.

REFERENCES

[1] Y.-Y. Zhang , Q.-X. Pei , Z.-D. Sha , Y.-W. Zhang, Phys. Lett. A **383**, 2821 (2019).
[2] K. S. Novoselov, V. I. Fal'ko, L. Colombo, P. R. Gellert, M. G. Schwab, and K. Kim, Nature, **490**, 192 (2012).
[3] C.-Z. Ning, Advanced Photonics **1**, 014002 (2019).
[4] S. Beniwal, J. Hooper, D. P. Miller, P. S. Costa, G. Chen, S.-Y. Liu, P. A. Dowben, E. C. H. Sykes, E. Zurek, A. Enders, ACS Nano **11** 2486 (2017).
[5] S. Shallcross, S. Sharma, E. Kandelaki, and O. A. Pankratov, Phys. Rev. B **81** 1 (2010).
[6] P. Giraud, "Study of the Electronic Structure of hexagonal Boron Nitride on Metals Substrates," Master Thesis, Université des Science et Technologies Lille 1 (2012).
[7] G. Fiori, A. Betti, S. Bruzzone, and G. Iannaccone, ACS Nano **6**, 2642 (2012).
[8] Q. Peng, S. De, Phyica E **44** 1662 (2012).
[9] J. Singh, "Electronic and optoelectronic properties of semiconductor structures," Cambridge University Press (2007).
[10] A. Mehdipour, K. Sasaoka, M. Ogawa and S. Souma, Jpn. J. Appl. Phys. **53**, 115103 (2014).